ISIJ International, Vol. 52 (2012), No. 10, pp. 1841–1847

Effects of Second Phase Particles on Migration of α/γ Interface during Isothermal α to γ Transformation

Liang CHEN,[1)]* Kiyotaka MATSUURA,[2)] Munekazu OHNO[2)] and Daisuke SATO[1)]

1) Graduate Student, Graduate School of Engineering, Hokkaido University, Kita 13 Nishi 8, Kita-ku, Sapporo, Hokkaido, 060-8263 Japan. E-mail: SATO_soshiki@frontier.hokudai.ac.jp
2) Division of Materials Science and Engineering, Faculty of Engineering, Hokkaido University, Kita 13 Nishi 8, Kita-Ku, Sapporo, Hokkaido, 060-8263 Japan. E-mail: matsuura@eng.hokudai.ac.jp, mohno@eng.hokudai.ac.jp

(*Received on March 13, 2012; accepted on May 30, 2012*)

The effects of insoluble particles on migration of ferrite (α)/austenite (γ) interface during isothermal α to γ transformation at 1 133 K have been studied by means of a model experiment using diffusion couple method and a multi-phase field simulation. It was found that the insoluble particles, ZrO_2 or TiO_2 particles, could retard the migration of α/γ interface. And the tendency that the retarding effect becomes stronger with higher volume fraction of TiO_2 particle was observed. However, the retarding effect of ZrO_2 on α/γ interface is not as strong as that on δ–ferrite (δ)/austenite (γ) interface during peritectic transformation. The phase field simulation indicates that this reduction of retarding effect originates from the appearance of carbon pile-up in γ phase, which is also caused by the existence of particles. In addition, it is shown that the difference between $\sigma_{\alpha/p}$ and $\sigma_{\gamma/p}$, the interfacial energy between matrix (α or γ) and particles, strongly affects the migration velocity of α/γ interface.

KEY WORDS: phase transformation; α/γ interface; second phase particle; pinning effect; diffusion couple; multi-phase field simulation.

1. Introduction

During the reheating process of carbon steels from room temperature, reaustenization occurs above eutectoid temperature from low temperature structures such as pearlite and martensite structures. It is important to refine the reversely-transformed austenite grain structure, since fine grain structures of reversely-transformed austenite lead to a refinement of the final structures (low temperature structures), such as ferrite, pearlite and martensite, which contributes to good mechanical properties for carbon steel.[1,2)] The microstructure of reversely-transformed austenite is strongly dependent on the kinetics of reverse transformation, which generally proceeds by nucleation and growth processes.[3,4)] It was reported that when the nucleation rate is high, the reversely-transformed austenite grains are refined.[5)] It is expected that if the growth process of austenite is retarded during the reverse transformation, the occurrence of nucleation event of austenite should be prompted. Hence, retardation of the growth of austenite is preferable for the purpose of obtaining fine austenite grain structure after the reverse transformation.

The reverse transformation has attracted the interest of many researchers. A variety of researches have been performed[5–19)] to clarify the mechanism and kinetics of reverse transformation. However, the early efforts mainly concentrated on the effects of initial microstructure, alloying elements and heating history on the kinetics of reverse transformation and little has been addressed regarding the retarding effect of insoluble particles on kinetics of reverse transformation, which is the main concern of the present study. The present work focuses on the reverse transformation from ferrite (α) to austenite (γ) transformation and the effects of insoluble particles such as ZrO_2 or TiO_2 particles on the migration of α/γ interface.

It is well known that the insoluble particles have significant retarding effect on grain growth,[20–23)] theoretical analysis of which was firstly given by Zener.[24)] In our recent study[25)] about the kinetics of peritectic transformation at 1 718 K in Fe–C alloy, it was found that the insoluble ZrO_2 particles existing in δ ferrite phase also retarded the migration of δ–ferrite (δ)/austenite (γ) interface. Although the driving force for δ/γ interface migration originates from the difference in the chemical potential between δ and γ phases, which is different from that of grain growth, the retarding effect also emerges because the migration of δ/γ interface passing over the particles involves the increase of the total amount of interfacial energy. According to these facts, the migration of α/γ interface during α to γ transformation is also expected to be retarded by the insoluble particle existing in α phase as similar to the phenomenon on δ/γ interface. It should be noted that the migration of α/γ interface is generally carbon diffusion-controlled. The carbon diffusion is much lower in α to γ transformation compared with those in peritectic transformation, which might yield a dif-

* Corresponding author: E-mail: chenliang@eng.hokudai.ac.jp
DOI: http://dx.doi.org/10.2355/isijinternational.52.1841

ference in the retarding effects of insoluble particles on the interface migration.

The main objective of this study is to investigate the effects of insoluble particles such as large ZrO_2 particle (r=15 μm) or small TiO_2 particle (r=2 μm) on the migration of α/γ interface during an isothermal α to γ transformation at 1 133 K. For this, we carried out a model experiment using a diffusion couple method and multi-phase field simulations. One will see that although the large ZrO_2 particles do not obviously influence the migration velocity of α/γ interface, small TiO_2 particles produce a notable retarding effect, which is enhanced by increasing volume fraction of TiO_2 particles. In the simulation work, it was found that a carbon pile-up occurs in γ phase due to the addition of particles and this pile-up reduces the retarding effect.

2. Experimental Procedures

A model experiment using a diffusion couple method was carried out to investigate the α to γ transformation. The diffusion couple consists of γ sample made by commercial S45C steel and α sample made by the mixture of pure iron powder and insoluble particles. When γ and α samples are held in contact with each other at 1 133 K, α to γ transformation takes place and the newly transformed γ phase appears on the interface between these two samples and grows into the α sample due to the carbon diffusion from the γ sample. Therefore, this model experiment enables us to investigate the migration of α/γ interface during this isothermal α to γ transformation in detail.

Figure 1 schematically represents the procedures for preparation of the diffusion couple sample. The mold and punches were machined from commercial S45C steel rods having diameters of 40 mm and 25 mm, respectively. Iron powder of 150 μm in diameter was mixed with ZrO_2 or TiO_2 particles by ball milling for 2 hrs. The powder mixture was put inside the S45C steel mold enclosed by two S45C steel punches and cold pressed at room temperature with a pressure of 870 MPa. Then, after the sample was heated to 1 073 K with a heating rate of around 80 K/min, the hot pressing was performed with a pressure of 230 MPa, followed by quenching. After these procedures, the $\gamma/\alpha/\gamma$ diffusion couple sample was prepared. The longitudinal section of the diffusion couple sample is schematically drawn in Fig. 1(b). The chemical compositions of S45C steel and the iron powder used in present study are listed in **Table 1**. One may notice that the S45C steel contains some amount of Si and Mn. It was reported[17] that the addition of Si and Mn slightly retarded the kinetics of reverse transformation by decreasing the carbon activity gradient. In the present discussion, however, the effects of Si and Mn on migration of α/γ interface are not explicitly taken into account for simplicity. The radius, r and volume fraction, f_v of the added spherical ZrO_2 particles were 15 μm and 0.10, respectively. For TiO_2 particles, the average radius was around 2 μm and the volume fraction was varied from 0.03 to 0.10.

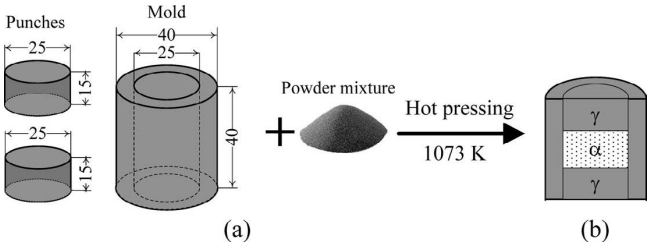

Fig. 1. Schematic drawing of (a) mold and punches produced from S45C steel rod and mixture of iron powder and insoluble particles and (b) longitudinal section of $\gamma/\alpha/\gamma$ diffusion couple sample after hot-pressing (unit: mm).

Table 1. Chemical compositions (wt%) of the S45C steel rod and iron powder.

	C	Si	Mn	P	S	Al	O	N	Fe
S45C	0.436	0.204	0.697	0.014	0.014	0.025	0.0015	0.0052	Bal.
Iron powder	–	0.010	0.010	0.002	0.002	0.001	–	–	Bal.

The prepared diffusion couple sample in a MgO crucible was then placed inside an electric furnace and was heated to experimental temperature 1 133 K with an average heating rate of around 40 K/min. The holding time at 1 133 K was varied from 6 to 24 hrs. During this heating and holding process, Nitrogen gas was flowing into the MgO crucible to avoid oxidation and a K-type thermocouple was inserted to the diffusion couple sample to have a precise temperature monitoring. When a predetermined holding time passed, the diffusion couple was rapidly dropped into iced water. The quenched sample was then sectioned in the longitudinal direction and etched by nital (3 vol%) solution after fine polishing. The microstructure examinations were performed by means of an optical microscope. Based on the optical microscope observation, the average thickness of newly transformed γ phase was measured.

3. Multi-Phase Field Model

In our recent study,[25] a phase field simulation was carried out based on the model proposed by Steinbach and Pezzola[26,27] to investigate the particle effects on migration of δ/γ and Liquid/γ interfaces during isothermal peritectic transformation. In the present study, to gain deeper insights about the experimental findings, we carried out a phase field simulation for α to γ transformation including dispersed particles at 1 133 K based on the model reported in Ref. 25). Moreover, as we mentioned, the effects of alloying elements in S45C steel on migration of α/γ interface are not explicitly taken into account for simplicity in the present study. The simulation is only focused on an Fe–C system. Here, the essential parts of the present phase field model are briefly summarized.

The existence of phase i is characterized by the order parameter ϕ_i, which continuously varies from 0 to 1. The subscript i specifies different phases and i=α, γ and p represent α, γ phases and insoluble particles, respectively. The normalization condition $\sum \phi_i = 1$ is held. In the present model, the carbon concentration, c, is given by, $c = \sum_{i=1}^{n} \phi_i c_i$, with the concentration associated with i phase, c_i.

The time evolution of order parameter, ϕ_i, is described by the following equation,

$$\frac{\partial \phi_i}{\partial t} = -\frac{2}{N}\sum_{j\neq i}^{n} s_{ij} M_{ij} \left\{ \sum_{j\neq i}^{n} \left[\frac{\varepsilon_{ij}^2}{2}\nabla^2\phi_j + \omega_{ij}\phi_j \right] - \sum_{i\neq j}^{n} \left[\frac{\varepsilon_{ij}^2}{2}\nabla^2\phi_i + \omega_{ij}\phi_i \right] + \frac{RT}{V_m}\left[(c_i - c_j) - (c_i^{e,j} - c_j^{e,i}) \right] \right\}, \quad \text{..... (1)}$$

where N is the number of coexisting phases at a given spatial point, s_{ij} takes 1 when i and j phases coexist and it takes 0 otherwise. ε_{ij} and ω_{ij} are respectively given in Eqs. (2) and (3). The third term of Eq. (1) is the driving force in dilute alloy system,[28] where R is gas constant, T is the temperature in Kelvin, V_m is molar volume and $c_i^{e,j}$ represents the concentration of i phase in equilibrium with j phase calculated by CALPHAD method . M_{ij} is the mobility of i/j interface given in Eq. (4).[29,30]

$$\varepsilon_{ij} = \frac{2}{\pi}\sqrt{2W\sigma_{ij}}\ , \quad \text{..... (2)}$$

$$\omega_{ij} = \frac{4\sigma_{ij}}{W}\ , \quad \text{..... (3)}$$

where σ_{ij} is the interfacial energy between i and j phases and W is the interface thickness.

$$M_{ij} = \left(\frac{15}{4}\frac{a\varepsilon_{ij}{}^2 RT_{m,ij}}{\omega_{ij} D_j}(1-k_{ij})(c_i^{e,j} - c_j^{e,i}) \right)^{-1}, \quad \text{..... (4)}$$

where a = 0.6276 and $T_{m,ij}$ is the transition temperature between i and j phases in pure iron.

The time evolution of carbon concentration, c, is described by the following equation,

$$\frac{\partial c}{\partial t} = \nabla \cdot \sum_{i=1}^{n} D_i \phi_i \nabla c_i = \nabla \cdot \sum_{i=1}^{n} D_i \phi_i k_{i\gamma} \nabla c_\gamma\ , \quad \text{..... (5)}$$

where D_i is diffusion coefficient in i phase, $k_{i\gamma}$ is the partition coefficient defined as $k_{i\gamma}$=c_i/c_γ.

The two-dimensional (2-D) phase field simulation system is illustrated in **Fig. 2**(a). The initial α/γ interface has a planar shape, which will be kept during the whole simulation process. For the sake of convenience, the area fraction of particles in 2-D is called as volume fraction, f_v, in 3-D. The Neumann boundary condition was applied to x direction and periodic boundary condition was applied to y direction. The length in x direction of initial γ and α phases is fixed to 100 μm and 50 μm, respectively, while the length in y direction is varied with the particle volume fraction. The spherical particles having a radius, r, of 0.5 μm are uniformly dispersed in α phase. By setting the interface mobility, $M_{\alpha/p}$, $M_{\gamma/p}$ to 0, the particle shape and position do not change and by setting the diffusion coefficient of particle D_p to 0, the carbon cannot diffuse into the particles. The initial carbon concentration profile was set according to the experimental condition as shown in Fig. 2(b). γ phase has a constant carbon concentration of 0.436 wt% (S45C steel), while there is no carbon in α phase (iron powder). At the α/γ interface, the local equilibrium condition is assumed, where carbon concentration changes continuously from $c_\gamma^{e,\alpha}$ to $c_\alpha^{e,\gamma}$. The parameters used in simulation are listed in **Table 2**. The values of interfacial energies between matrix (α or γ) and particles, $\sigma_{p/\alpha}$ and $\sigma_{p/\gamma}$, were assumed, because the values were not reported.

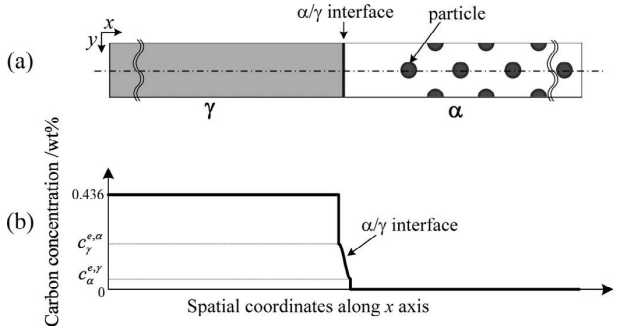

Fig. 2. Schematic drawing of (a) phase field simulation system and (b) initial carbon concentraion profile along the center line indicated in (a).

It is noted that the present simulations provide only qualitative results as detailed below. The present multi-phase field model suffers from anomalous interface effects.[28] In order to save the computational time, the simulations were restricted to 2-D system and the system size and the particle size were also limited to be small compared to the experimental condition. In addition, there are the uncertainty in the values of $\sigma_{\alpha/p}$ and $\sigma_{\gamma/p}$. Hence, the present simulations do not provide quantitatively meaningful results. However, they can be used to get qualitative information that should be helpful to better understand our experimental findings.

4. Results and Discussion

The longitudinal section of the sample having ZrO_2 particles with r=15 μm and f_v=0.10 is shown in **Fig. 3**. Figure 3(a) shows the initial microstructure in the sample quenched after hot-pressing at 1 073 K. One can see that spherical ZrO_2 particles are dispersed in α sample and there is no pore or crack near initial α/γ interface, which is indicated by the arrow on the left side of Fig. 3(a). The initial microstruc-

Table 2. Parameter values used in present simulation.

Parameter	Symbol	Value (unit)
system size	–	150×l (μm^2) (l: inter-particle spacing)
mesh size	Δx	10^{-7} (m)
	Δy	10^{-7} (m)
time step	Δt	5.0×10^{-6} (s)
interface width	W	7.0×Δx (m)
molar volume	V_m	7.7×10^{-6} (m^3 mol^{-1})
interfacial energy[31–33]	$\sigma_{\alpha/\gamma}$	1.0 (J m^{-2})
	$\sigma_{\alpha/p}$	1.0 (J m^{-2})
	$\sigma_{\gamma/p}$	1.0 (J m^{-2})
diffusion coefficient[31]	D_γ	$1.50\times10^{-5}\exp(-14.20\times10^4/RT)$ (m^2 s^{-1})
	D_α	$2.20\times10^{-4}\exp(-12.25\times10^4/RT)$ (m^2 s^{-1})
	D_p	0 (m^2 s^{-1})
$i\rightarrow j$ phase transition temperature of pure iron	$T_{m,a\gamma}$	1 185 (K)

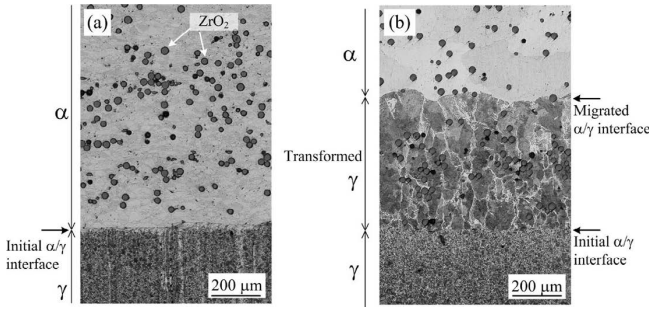

Fig. 3. Microstructures on the longitudinal section of sample having ZrO_2 particles with r=15 μm and f_v=0.10, quenched after (a) hot-pressing at 1 073 K and (b) holding at 1 133 K for 24 hrs.

tures of α and γ samples are fine equiaxed α grains and fine pearlite structure at room temperature, respectively. Figure 3(b) shows the microstructure of the sample quenched after holding at 1 133 K for 24 hrs. It is easily recognized that the newly transformed γ phase having coarse columnar γ grains appears between initial α and γ phases. Since both of the initial and migrated α/γ interfaces can be clearly identified as indicated on the right side of Fig. 3(b), the thickness of newly transformed γ phase can be measured. It should be noted that the α/γ interface is slightly curved in the experimental sample due to the multi-grain structures in γ phase. Such an effect might be important on the migration of α/γ interface but beyond the scope of this study, so the planar α/γ interface was assumed in our phase field simulation as mentioned above, to only focus on the most essential behavior of the particle retarding effect.

Figure 4 shows the thickness of transformed γ phase with respect to holding time in samples without and with ZrO_2 particles of r=15 μm and f_v=0.10. It can be seen that the thickness of transformed γ phase linearly increases with square root of holding time in each sample, following a parabolic growth law. Although the thickness in samples having ZrO_2 particles is always smaller than that in samples without particle in each time period, the difference between them is quite small, which indicates a very small retarding effect on α/γ interface migration. However, in our study about peritectic transformation,[25] it was shown that the same radius and volume fraction of ZrO_2 particles in δ phase produce a significant retarding effect on the migration of δ/γ interface. The reason for this difference will be discussed later. For a further study, fine TiO_2 particles having a smaller average radius of around 2 μm were used as insoluble particle. The result for fine TiO_2 particles is shown in **Fig. 5**. It is found that the thickness of transformed γ phase decreases by the addition of fine TiO_2 particles, especially in case of f_v=0.10. Namely, TiO_2 particles have obvious retarding effect on α/γ interface.

As shown in Figs. 4 and 5, the growth of transformed γ phase obeys a parabolic law described as,

$$x = a_{\alpha/\gamma}\sqrt{t} \quad \text{..... (6)}$$

where x (μm) is the thickness of γ phase, t (s) is the holding time and $a_{\alpha/\gamma}$ (μm/s$^{1/2}$) is the so-called parabolic constant for α/γ interface. In this paper, the value of $a_{\alpha/\gamma}$ is used as a measure of the velocity of α/γ interface. The value of $a_{\alpha/\gamma}$ regressed from the experimental data is shown in **Fig. 6**. By

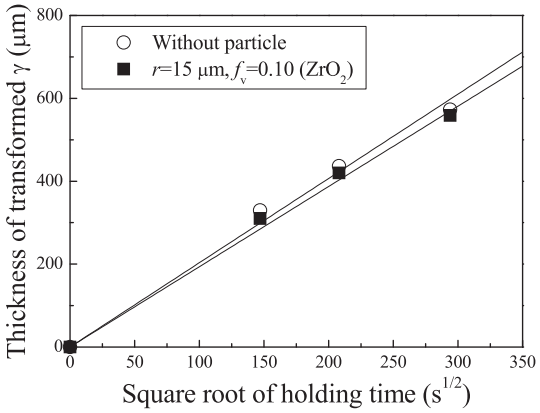

Fig. 4. Thickness of newly transformed γ phase with varied holding time at 1 133 K in samples without and with ZrO_2 particles with r=15 μm, f_v=0.10.

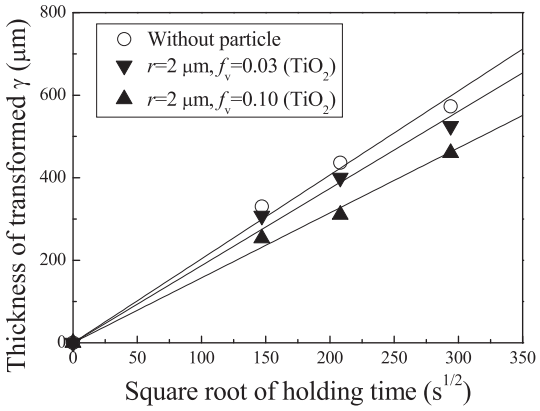

Fig. 5. Thickness of newly transformed γ phase with varied holding time at 1 133 K in samples without and with TiO_2 particles with r=2 μm, f_v=0.03 and 0.10.

comparing the value of $a_{\alpha/\gamma}$ in samples with and without particles, it is clear that large ZrO_2 particles have slight retarding effect, while fine TiO_2 particles have obvious retarding effect. Moreover, the retarding effect of TiO_2 on α/γ interface becomes significant with higher f_v. This experimental finding can be qualitatively explained according to the Zener equation that the pinning pressure P_Z on α/γ interface due to all particles in unit area, which is estimated as,[34]

$$P_Z = \frac{3 f_v \sigma_{\alpha/\gamma}}{2r} \quad \text{..... (7)}$$

where $\sigma_{\alpha/\gamma}$ is the interfacial energy of α/γ interface. Particles with higher f_v generate a stronger pinning pressure and hence enhance the retarding effect.

As mentioned above, it was observed that retarding effect of ZrO_2 particles on α/γ interface is quite small, which is in contrast to the strong retarding effect observed for δ/γ interface migration. To clarify the possible reasons for this point and also to confirm the validity of the experimental findings, we performed the phase field simulation. The simulated results are discussed as follows.

The migration behavior of α/γ interface at different time steps is shown in **Fig. 7**. The samples without and with particles of r=0.5 μm and f_v=0.20 are compared. In the sample without particles, α/γ interface keeps planar shape during the whole transformation. However, in the sample with par-

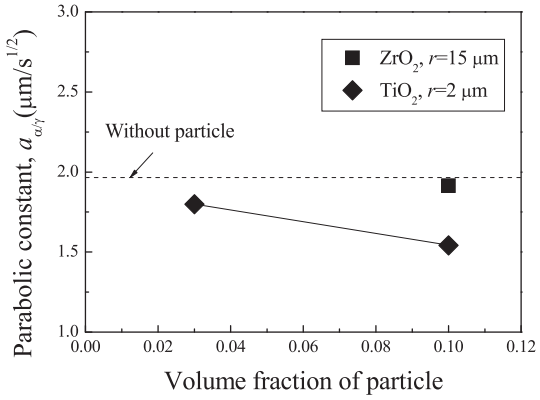

Fig. 6. Parabolic constants of α/γ interface regressed from experimental results.

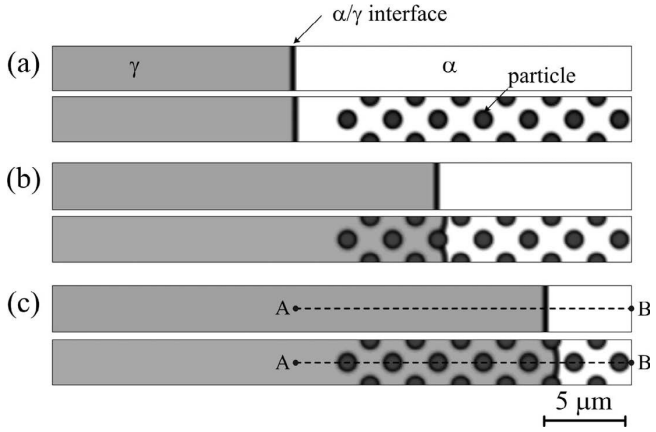

Fig. 7. Migration behavior of α/γ interface compared in samples without and with particles (r=0.5 μm, f_v=0.20) at different time steps of (a) t=0, (b) t=22.5 s and (c) t=56.0 s. Grey area, bright area and black circular area correspond to γ, α phases and particles, respectively. (The dashed lines AB in (c) will be used to discuss the carbon concentration along them later.)

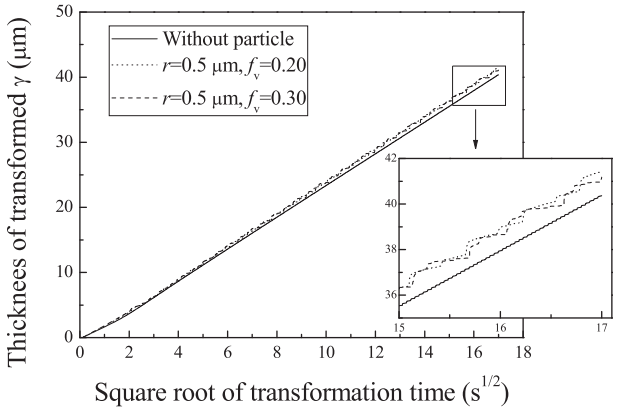

Fig. 8. Time dependences of thickness of newly transformed γ phase in samples without and with particles obtained from simulation ($\sigma_{\alpha/\gamma}/\sigma_{\alpha/p}/\sigma_{\gamma/p}$=1.0/1.0/1.0 J/m^2). The enlarged figure corresponds to the indicated rectangle area.

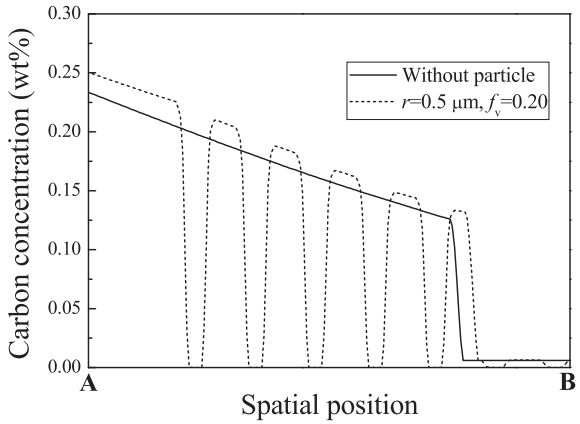

Fig. 9. Carbon concentration profile in samples without particle and having particles with r=0.5 μm and f_v=0.20 at time step of 56.0 s along the dashed lines shown in Fig. 7(c).

ticles, α/γ interface is bent when it meets a particle as shown in Figs. 7(b) and 7(c). In the case of $\sigma_{\alpha/p}=\sigma_{\gamma/p}$ assumed in the simulation, the change of total amount of interfacial energy in this 2-D system only depends on the length change of α/γ interface. The 'bent' process involves increasing length of α/γ interface due to the change of its shape and increases the total amount of interfacial energy. Therefore, α/γ interface should migrate slowly when it passes over particles. However, from **Fig. 8** showing the time dependency of growth of transformed γ phase, the retarding effect is not observed, even when f_v=0.30. To clarify the reason, the carbon concentration along the dashed line indicated in Fig. 7(c) is investigated and plotted in **Fig. 9**. It is obvious that the carbon concentration in γ phase is higher in sample with particles than that in without particle sample. This phenomenon occurs because particles block carbon diffusion from γ phase to α phase due to the low carbon diffusivity for α to γ transformation at 1 133 K. The pile-up of carbon increases the concentration gradient in γ phase near α/γ interface, which accelerate the carbon diffusion in γ phase. Hence, the migration velocity of α/γ interface is thus accelerated, since it is controlled by the carbon diffusion in γ phase. It is true that particles have pinning force when the 'bent' α/γ interface passes over particles as discussed above, which will be called 'pinning force effect' hereafter. On the other hand, the pile-up of carbon causes faster carbon diffusion and accelerates the migration of α/γ interface, which will be called 'carbon pile-up effect' hereafter. These two opposite effects counteract each other.

Back to the experimental result, the finding that retarding effect of ZrO_2 particle is small for α/γ interface but significant for δ/γ interface is explained as follows. The migration of δ/γ interface proceeds at 1 718 K during peritectic transformation.[25] The carbon diffusion in γ phase for α to γ transformation is much slower than that for peritectic transformation, since the carbon diffusion coefficient, D_γ, is 2 orders magnitude lower. During such a slow diffusion process, it becomes difficult for carbon to bypass the particles, where the carbon cannot diffuse into. Hence, more carbon is blocked by the particles resulting in a stronger carbon pile-up effect for α to γ transformation compared with that for peritectic transformation. Under this circumstance, the pinning force effect on α/γ interface is counterbalanced by a stronger carbon pile-up effect and a slighter retarding effect is shown. One important aspect needed to be pointed out here is that the carbon pile-up effect should be much overestimated in the 2-D simulation. One can consider that, if the 2-D model shown in Fig. 2 is expanded to 3-D, the particle area with circle shape will become to round bar

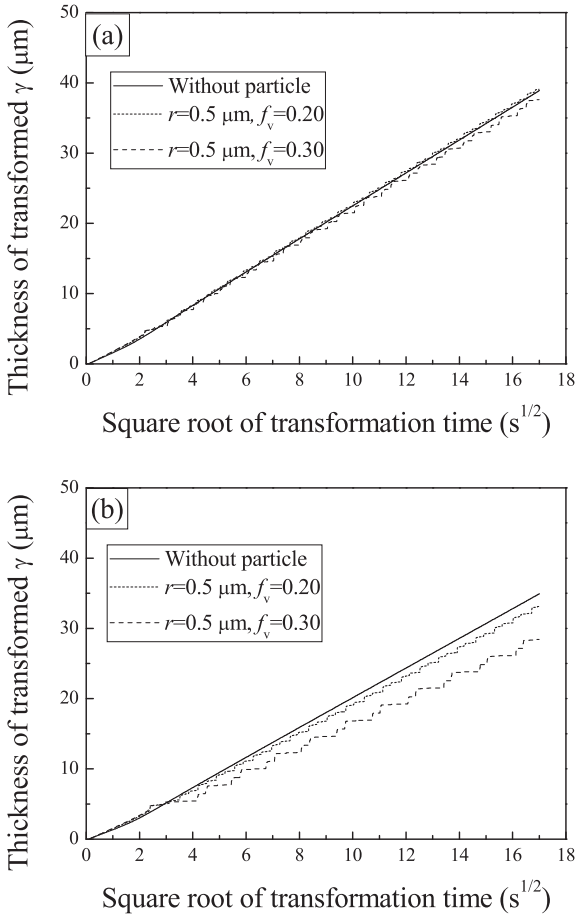

Fig. 10. Time dependences of thickness of transformed γ phase obtained from simulation using higher interfacial energy, $\sigma_{\alpha/\gamma}$: (a) $\sigma_{\alpha/\gamma}/\sigma_{\alpha/p}/\sigma_{\gamma/p}$=1.8/1.0/1.0 J/m^2 (b) $\sigma_{\alpha/\gamma}/\sigma_{\alpha/p}/\sigma_{\gamma/p}$= 4.0/1.0/1.0 J/m^2.

rather than spherical particle, which could strongly block the carbon diffusion. In the experimental condition, the carbon pile-up should occur but not as strong as that appeared in the simulation.

It is natural to consider that if the particle pinning force is large enough, the retarding effect becomes obvious even with the counterbalance of carbon pile-up, as the experimental result for fine TiO_2 particles shown in Fig. 5. In general, fine TiO_2 particles brought strong pinning force due to its smaller size according to Eq. (7). Therefore, to confirm this experimental result, a smaller particle should be introduced to the simulation to simulate the case with strong pinning force. However, in present simulation model, the minimum radius of particle we could try is 0.35 μm. It seems not small enough to achieve a stronger pinning force. According to Eq. (7), a strong pinning force also corresponds to a higher interfacial energy of α/γ interface, $\sigma_{\alpha/\gamma}$. So, the higher $\sigma_{\alpha/\gamma}$, 1.8 J/m^2 and 4.0 J/m^2 were tried to introduce a much stronger pinning force. Although the values of 1.8 J/m^2 and 4.0 J/m^2 seem to be too high compared with the realistic value, it can be used to overcome the overestimated carbon pile-up effect in 2-D simulation mentioned above. **Figure 10** shows the change of thickness of transformed γ phase with time in case of higher $\sigma_{\alpha/\gamma}$. From Fig. 10, one can find that, when pinning force is large enough, the retardation on α/γ interface becomes significant, indicating that the carbon pile-up effect is completely counterbalanced and the pinning force effect

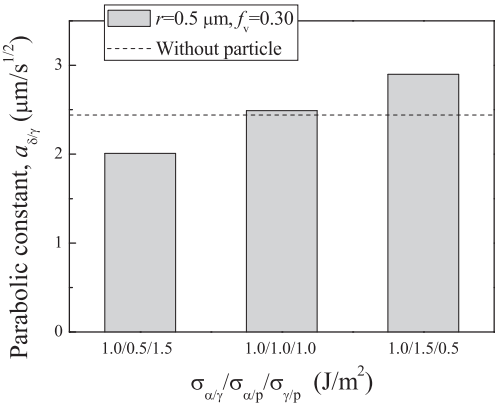

Fig. 11. Effect of unequal $\sigma_{\alpha/p}$ and $\sigma_{\gamma/p}$ on parabolic constants with a fixed $\sigma_{\alpha/\gamma}$=1.0 J/m^2 in sample having particles with r=0.5 μm and f_v=0.30. The dashed line shows the case of without particle for a comparison.

becomes the dominated factor. Therefore, by this indirect way, it was proved that the fine TiO_2 particles having strong pinning force could effectively retard α/γ interface, since the carbon pile-up effect is completely counterbalanced by the strong pinning force. Additionally, when the retarding effect is obvious as shown in Fig. 10(b), the retarding effect becomes significant with increase of particle volume fraction, which is consistent with the experimental result about different f_v of TiO_2 particles shown in Fig. (5).

The effect of interfacial energy between matrix (α or γ) and particles, $\sigma_{\alpha/p}$ and $\sigma_{\gamma/p}$, on velocity of α/γ interface is discussed. Generally, the value of $\sigma_{\alpha/p}$ and $\sigma_{\gamma/p}$ should not be equal. Since no exact value was reported for interfacial energy between matrix and ZrO_2 or TiO_2 particles, $\sigma_{\alpha/p}$ and $\sigma_{\gamma/p}$ were assumed to be equal in above simulation. Here, the simulation with unequal values between $\sigma_{\alpha/p}$ and $\sigma_{\gamma/p}$ but with a fixed value of $\sigma_{\alpha/\gamma}$ of 1.0 J/m^2 is carried out in sample having particles with r=0.5 μm and f_v=0.30. **Figure 11** shows the parabolic constant affected by varied values of $\sigma_{\alpha/p}$ and $\sigma_{\gamma/p}$. By comparing with the case without particle, it can be seen that, when $\sigma_{\alpha/p}<\sigma_{\gamma/p}$, α/γ interface is significantly retarded, however, when $\sigma_{\alpha/p}>\sigma_{\gamma/p}$, α/γ interface is even accelerated. If $\sigma_{\alpha/p}<\sigma_{\gamma/p}$, the increment of total amount of interfacial energy occurs, since the length of γ/p interface increases when α/γ interface passes over particles and hence it retards its migration. On the other hand, if $\sigma_{\alpha/p}>\sigma_{\gamma/p}$, the decrease of total amount of interfacial energy occurs when α/γ interface passes over particles, which enhances the velocity of α/γ interface. Although this point cannot be used to discuss present experimental results due to unknown $\sigma_{\alpha/p}$ and $\sigma_{\gamma/p}$, we claim that it should be a factor which affects the strength of particle retarding effect on α/γ interface.

5. Conclusion

The effects of second phase particles on migration of α/γ interface during isothermal α to γ transformation at 1 133 K were studied by means of a model experiment and multi-phase field simulations. Some results are compared with our recent study about migration of δ/γ interface during peritectic transformation.[25] It was found that the strength of retarding effect on α/γ interface depends on several factors, such as the pinning force, carbon pile-up effect and the interfacial

energy between matrix and particles. The important results are listed as follows.

(1) From the experimental results, it was found that large ZrO_2 particles have small retarding effect on α/γ interface migration, which is not as strong as that on δ/γ interface, while for fine TiO_2 particles, the retarding effect becomes obvious and increases with higher particle volume fraction.

(2) Based on the carbon profile derived from simulation, carbon pile-up with addition of particles in γ phase is found. This carbon pile-up effect explains the reduction in strength of retarding effect on α/γ interface mentioned in conclusion (1).

(3) The simulations showed that if the particle pinning force is strong enough, the retarding effect on α/γ interface becomes obvious. And the retarding effect becomes significant with increases in particle volume fraction, which is in agreement of the experimental findings.

(4) The difference between interfacial values of $\sigma_{\alpha/p}$ and $\sigma_{\gamma/p}$ affects velocity of α/γ interface. When $\sigma_{\alpha/p}<\sigma_{\gamma/p}$, the α/γ interface is strongly retarded, however, when $\sigma_{\alpha/p}>\sigma_{\gamma/p}$, α/γ interface is even accelerated.

REFERENCES

1) T. Furuhara, K. Kikumoto, H. Saito, T. Sekine, T. Ogawa, S. Morito and T. Maki: *ISIJ Int.*, **48** (2008), 1038.
2) H. Sekine and T. Maruyama: *Trans. Iron Steel Inst. Jpn.*, **16** (1976), 427.
3) R. A. Roberts and R. F. Mehl: *Trans. AIME*, **31** (1943), 613.
4) C. R. Brooks: Principles of the Austenitization of Steels, Elsevier Applied Science, London, UK, (1992), 81.
5) J. Syarif and Z. Sajuri: *Sains Malaysiana*, **39** (2010), No. 6, 999.
6) M. Nemoto: *Metall. Trans. A*, **8A** (1977), 431.
7) G. R. Speich, V. A. Demarest and R. L. Miller: *Metall. Trans. A*, **12A** (1981), 1419.
8) L. Karmazin: *Mater. Sci. Eng.*, **A142** (1991), 71.
9) T. Akbay, R. C. Reed and C. Atkinson: *Acta Metall. Mater.*, **42** (1994), 1469.
10) L. Karmazin and J. Krejčí: *Mater. Sci. Eng.*, **A185** (1994), L5.
11) T. Akbay and C. Atkinson: *J. Mater. Sci.*, **31** (1996), 2221.
12) R. C. Reed, T. Akbay, Z. Shen, J. M. Robinson and J. H. Root: *Mater. Sci. Eng.*, **A256** (1998), 152.
13) Y. I. Son, Y. K. Lee and K. T. Park: *Metall. Mater. Trans. A*, **37A** (2006), 3161.
14) K. T. Park, E. G. Lee and C. S. Lee: *ISIJ Int.*, **47** (2007), 294.
15) S. J. Lee and Y. K. Lee: *Mater. Des.*, **29** (2008), 1840.
16) G. Miyamoto, Z. D. Li, H. Usuki and T. Furuhara: *Mater. Sci. Forum*, **638–642** (2010), 3400.
17) G. Miyamoto, H. Usuki, Z. D. Li and T. Furuhara: *Acta Mater.*, **58** (2010), 4492.
18) Z. D. Li, G. Miyamoto, Z. G. Yang and T. Furuhara: *Metall. Mater. Trans. A*, **42A** (2011), 1586.
19) J. Rudnizki, B. Böttger, U. Prahl and W. Bleck: *Metall. Mater. Trans. A*, **42A** (2011), 2516.
20) S. Morioka and H. Suito: *ISIJ Int.*, **48** (2008), 286.
21) A. V. Karasev and H. Suito: *ISIJ Int.*, **46** (2006), 718.
22) J. Janis, K. Nakajima, A. Karasev, H. Shibata and P. G. Jönsson: *J. Mater. Sci.*, **45** (2009), 2233.
23) M. Apel, B. Böttger, J. Rudnizki, P. Schaffnit and I. Steinbach: *ISIJ Int.*, **49** (2009), 1024.
24) C. S. Smith: *Trans. AIME*, **175** (1948), 15.
25) L. Chen, K. Matsuura, D. Sato and M. Ohno: *ISIJ Int.*, **52** (2012), 434.
26) I. Steinbach and F. Pezzolla: *Physica D*, **134** (1999), 385.
27) J. Tiaden, B. Nestler, H. J. Diepers and I. Steinbach: *Physica D*, **115** (1998), 73.
28) S. G. Kim, W. T. Kim and T. Suzuki: *Phys. Rev. E*, **60** (1999), 7186.
29) M. Ohno and K. Matsuura: *Acta Mater.*, **58** (2010), 6134.
30) M. Ohno and K. Matsuura: *Acta Mater.*, **58** (2010), 5749.
31) K. Nakajima, M. Apel and I. Steinbach: *Acta Mater.*, **54** (2006), 3665.
32) I. Loginova, J. Odqvist, G. Amberg and J. Ågren: *Acta Mater.*, **51** (2003), 1327.
33) C. J. Huang, D. J. Browne and S. McFadden: *Acta Mater.*, **54** (2006), 11.
34) P. A. Manohar, M. Ferry and T. Chandra: *ISIJ Int.*, **38** (1998), 913.